Taylor & Francis
Taylor & Francis Group

Automatika

Journal for Control, Measurement, Electronics, Computing and Communications

ISSN: (Print) (Online) Journal homepage: www.tandfonline.com/journals/taut20

Design of Z source converter with the genetic-based chicken swarm algorithm for closed loop control of PV integrated grid

R. Aandal & A. Ravi

To cite this article: R. Aandal & A. Ravi (2024) Design of Z source converter with the genetic-based chicken swarm algorithm for closed loop control of PV integrated grid, Automatika, 65:3, 675-690, DOI: 10.1080/00051144.2024.2308463

To link to this article: https://doi.org/10.1080/00051144.2024.2308463

Published online: 15 Feb 2024.

AUTOMATIKA
2024, VOL. 65, NO. 3, 675–690
https://doi.org/10.1080/00051144.2024.2308463

Design of Z source converter with the genetic-based chicken swarm algorithm for closed loop control of PV integrated grid

R. Aandal and A. Ravi

EEE Department, Francis Xavier Engineering College, Tirunelveli, India

ABSTRACT

A single-phase grid coupled PV system with a switched Z-source boost converter is analysed on the basis of closed-loop control using a novel hybrid algorithm. As PV results in low-voltage DC, it is vital to step up this low-voltage DC and so a suitable DC-DC converter is needed. A switched Z-source boost converter is utilized for the step-up process as this converter uses minimum passive components, thereby reducing the cost with improved power density. Control of the converter is carried out by a closed loop control using a PI controller tuned with a novel genetic-based chicken swarm (GBCS) algorithm which combines the merits of both genetic and chicken swarm able to deal with complex problems, simple with fast convergence. The output of the converter is then given to the grid through a single-phase VSI in which DC–AC conversion takes place. While connecting PV to the grid, another factor to be taken care of is grid synchronization which is accomplished by a PI controller in which the actual and reference power are analogized. The proposed control scheme is simulated in a MATLAB environment and the outcomes are observed. The grid current THD of 1.6% and reactive power compensation is accomplished.

ARTICLE HISTORY
Received 25 July 2022
Accepted 17 January 2024

KEYWORDS
Genetic-based chicken swarm algorithm; PV system; switched Z-source boost converter; grid synchronization

1. Introduction

Nowadays, there is an urge to overcome the increasing deterioration of the environmental conditions and so the countries in the world are forced towards renewable energy resources [1]. Among the renewable energy source and electrical grid network, the interconnections are performed with the distributed generation, where the important tasks are performed by the power electronics [23]. Generally, photovoltaic (PV) systems are classified into standalone and grid-connected types, in which most of the PV solar power systems are connected to the grid [4]. Every country uses a different system type and different characteristics of grid; however, most of the PV inverter systems are coupled with low-voltage (LV) or medium-voltage (MV) [5]. The code certifications of LV and MV are the major issues in PV inverter systems, also the dynamic power from the PV array is supplied towards the grid because the PV system uses a current control scheme [6]. Generally, the power plants are coupled with the LV or MV, this contributes the grid stability and also the power plant generation is achieved by current control which contains a few weak points during execution [7]. The variation of grid frequency is considered by controlling the active power and because of high penetration, the grid instability is prevented. If the variation of grid voltage is greater than 10%, then it causes voltage sag and if it is less than 10%, it causes voltage swell [8]. To achieve these issues, grid-oriented PV inverter systems should supply power in active power through maximum power tracking and also through reactive power grid for code certifications [9].

The converters used in PV are Boost, SEPIC, LUO and Z-source converters, among this the most commonly used converter is the boost converter [10] which steps up the input voltage by utilizing the level of load. It stores energy in the inductor and supplies it to the load, this is a distinct capacity; however; the output voltage is maintained steadily with a large amount of capacitor values and causes large voltage stress [11]. The issues in the boost converter are addressed by utilizing the buck-boost converter [12], which controls the voltage for the variance in both irradiance and temperature. This converter results in discontinuous current output and requires large filter sizes and complex sensing circuits. The issues in these boost converters are achieved by the SEPIC converter [13], which performs both the buck and boost operations and the input required for this converter is in the form of radiation. This converter is not used in low-varying applications, so the LUO converter is utilized. The PV output voltage is boosted by the design of the LUO converter [14] and the implementation of this converter is expensive and its efficiency is low. The issues in this converter are rectified by the Z-source converter [15] which is coupled among the main circuit and power sources and performs both buck and boost operations. In [16], a multi-input single output (MISO) converter is utilized, which

CONTACT R. Aandal aandal1990@gmail.com EEE Department, Francis Xavier Engineering College, Tirunelveli, 627003, India

combines different distribution generation sources to achieve higher output voltage. Because of the natural conditions, the supply of the converter is stopped, to overcome these issues, a module-integrated converter (MIC) is used. This MIC converter [17] recycles the stored energy from the inductance and achieves maximum step-up output voltage and this converter requires only PV as a power source. In [18], a medium voltage distribution network converter (MVDC) is utilized because it contains a wide range of input voltage and it also needs high output voltage to achieve the MVDC requirements. In this developed paper, a switched Z-source boost converter is utilized to overcome these issues.

The maximum power point (MPP) is extracted from PV by using maximum power point tracking (MPPT). The MPPT [19] is used to obtain fast and accurate tracking and the system oscillation occurs due to different environmental conditions. However, the above-mentioned method for MPPT is accurate, but it creates some oscillation, to neglect these issues closed-loop control is employed with the PI controller. If the PI controller is used individually, then the settling time is increased and also the peak overshoot problems occur. To eliminate these issues, the PI controller is tuned using various algorithms such as fuzzy, PSO and genetic algorithms. Initially, the fuzzy algorithm [20] is utilized, based on the current operating condition of the control system. Tha PI controller is tuned by the fuzzy and it is unable to provide machine learning capability. To eliminate these issues, a hybrid algorithm named genetic-based chicken search algorithm is utilized in this work.

2. Proposed control scheme

The proposed control scheme for grid-connected PV with a switched Z-source boost converter using a genetic-based-chicken swarm algorithm is illustrated in Figure 1. PV modules usually result in low-voltage DC and it is necessary to boost this voltage. Hence a suitable converter is required for boosting the PV voltage.

A switched Z-source boost converter is utilized in this work which is constructed by adding a switch and a diode to the conventional Z-source converter. This converter steps up the attained PV voltage and the converter must be controlled. So, a closed-loop control is implemented with a PI controller and tuning of the controller is accomplished by a hybrid algorithm. A genetic-based chicken swarm algorithm is utilized for attaining the optimal parameters for the controller. In the GBCS algorithm, the population is initialized followed by the evaluation of fitness value and then the population is categorized into two. Using GA, one of the subpopulations is updated while the other is updated by the CS algorithm. Both solutions are combined for the next generation to achieve optimal solutions. Thus, the required pulses for the converter are generated with the aid of a PWM generator and the PI controller is tuned with the GBCS algorithm. For all the grid-connected PV systems, grid synchronization is a vital part and this is achieved by a PI controller in which the actual and

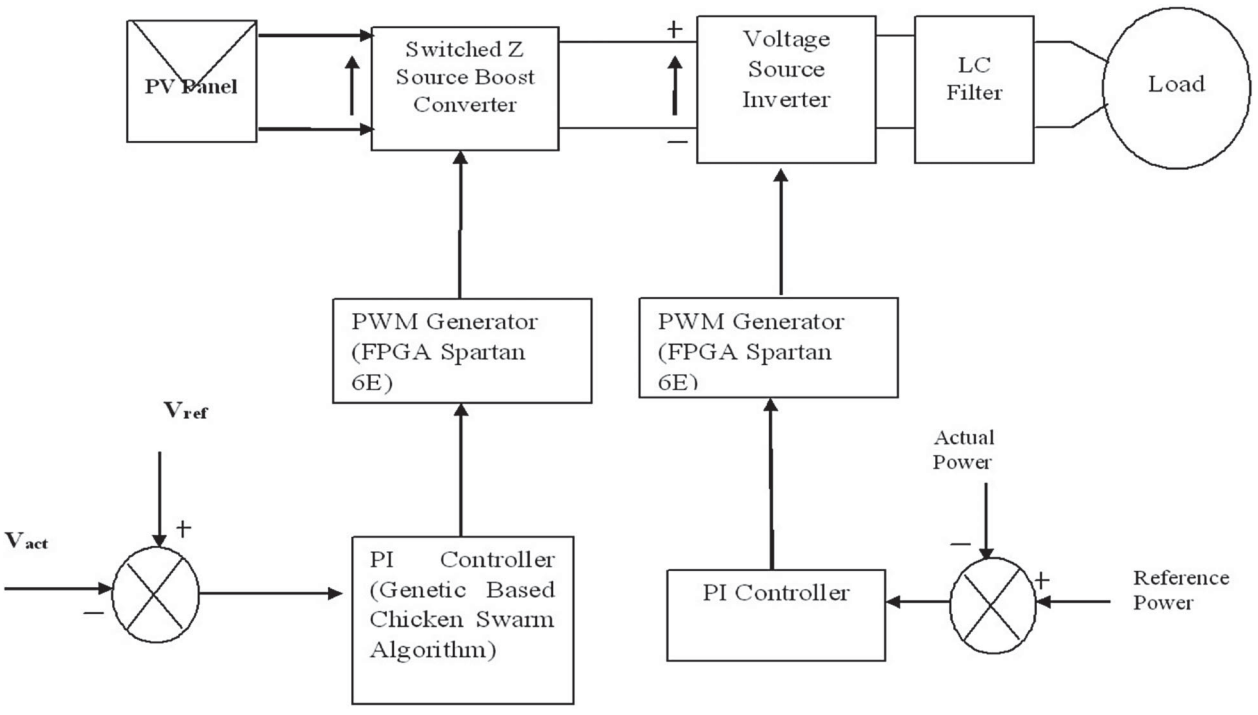

Figure 1. Proposed control scheme.

reference values of power are analogized and accordingly, pulses are generated for the single-phase VSI.

Switched Z-source DC-DC converter

A switched Z-source DC-DC converter (SZSC) is FS in Figure 2. Compared to the traditional circuit, the proposed circuit has one more switch (S_2) and diode (D_3). The boost factor of SZSC is enhanced, which is given by the relation $\frac{1}{(1-4D)}(0 < D < 0.25)$. The relationship between the boost factor and duty cycle is shown in Figure 2, to further illustrate the boost ability of the proposed converter. It is clear from this relationship that the proposed converter shows a higher boost ability than all other Z-source converters in a comparable frame. The proposed converter's highest operating duty cycle is D $<$ 0.25.

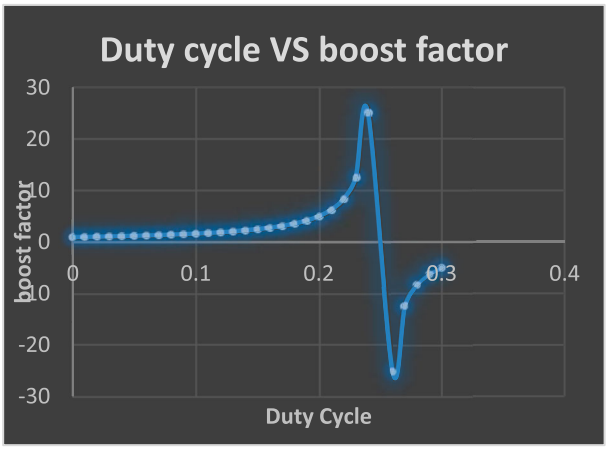

Figure 2. Duty cycle vs boost factor.

This converter operates in both continuous current mode (CCM) and discontinuous current mode (DCM). In a complete cycle, every mode has various circuit states. Figure 3 represents the circuit diagram of specifications of reference directions.

Operation of SZSC

The circuits for various modes are represented in Figure 3. Mode 1 has states 1 and 2, Mode 2 has states 1, 2 and 3 and Mode 3 has states 1, 2, 3 and 4. For easy analysis presumed all the components of power as ideal, free-wheeling diodes for switches S_1 and S_2 are neglected, inductances $L_1 = L_2$ and capacitances $C_1 = C_2$.

Mode 1 in CCM

Mode 1 has State 1 and 2 and

State 1$[t_0, t_1]$: When the switches S_1 and S_2 are concurrently ON, and diodes D_1, D_2 and D_3 are OFF, so current through these diodes is $i_{D_1} = i_{D_2} = i_{D_3} = 0$. C_1, C_2 and C_3 capacitors are discharged, whereas L_1 and L_2 inductors store energy, and the stored energy in the C_3 capacitor is moved to the load.

As shown in Figure 4 the capacitor C_1 and the inductor L_1 currents are equal from the current loop which is named$i_{C_1} = i_{L_1}$, the capacitor C_2 and the inductor L_2 currents are equal from the current loop which is named $i_{C_2} = i_{L_2}$ and switches S_1 and S_2 have equal currents which is named $i_{S_1} = i_{S_2}$. The state 1 equations are expressed as

$$\{i_{S_1} = i_{L_1} + i_{L_2} i_{C_3} = i_{S_1} + i_o \tag{1}$$

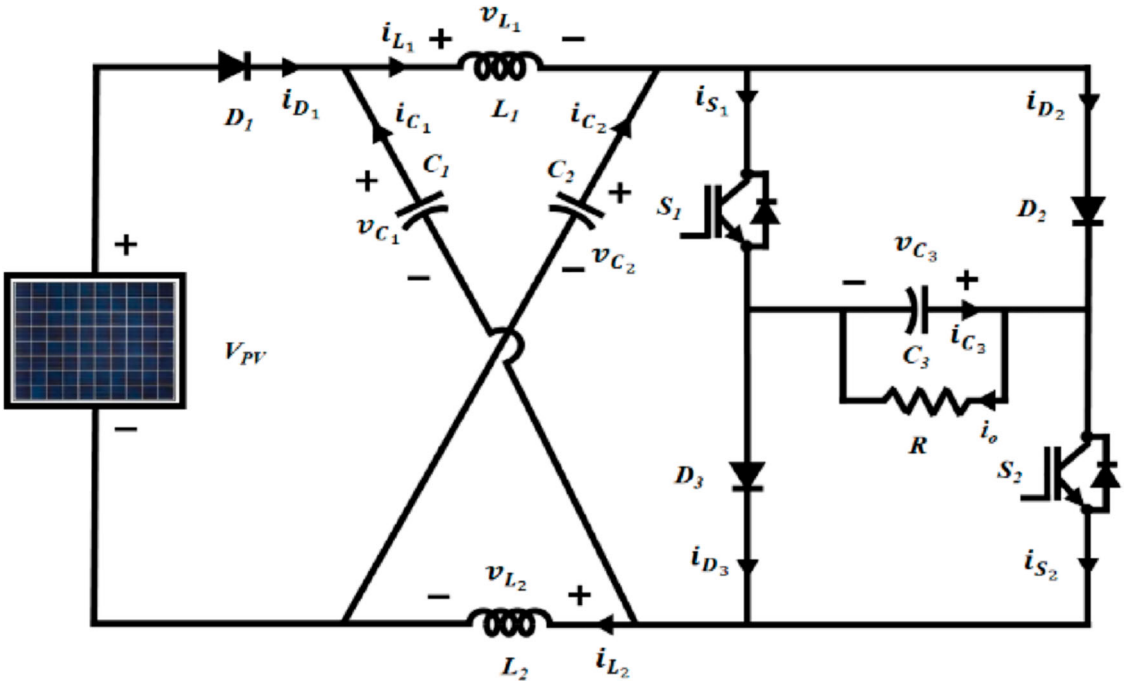

Figure 3. Circuit diagram of specifications of reference directions.

$$\{v_{L_1} = v_{C_1} + v_{C_3} v_{L_2} = v_{C_2} + v_{C_3} \quad (2)$$

State 2$[t_1, t_2]$: When the switches S_1 and S_2 are concurrently *OFF*, current through these switches is $i_{S_1} = i_{S_2} = 0$ and diodes D_1, D_2 and D_3 are *ON*. The V_{PV} panel voltage and the L_2 inductor discharge the energy to the C_1 capacitor, the V_{PV} panel voltage and the L_1 inductor discharge the energy to the C_2 capacitor and the V_{PV} panel voltage and the L_1 and L_2 inductors discharge the energy to the C_3 capacitor as well as the load. The circuit diagram for the current loop in state 2 is shown in Figure 5.

Apply KCL in Figure 4

$$\{i_{D_1} = i_{L_1} - i_{C_1} i_{D_2} = i_{L_1} + i_{C_2} i_{D_3} = i_o - i_{C_3} \quad (3)$$

Applying KVL in Figure 5

$$\{v_{C_1} = V_{PV} - v_{L_2} v_{C_2} = V_{PV} + v_{L_1} v_{C_3} = V_{PV} - v_{L_1} - v_{L_2} \quad (4)$$

The symmetry of the Z-source network is attained on both sides

$$\{i_{L_1} = i_{L_2} v_{L_1} = v_{L_2} i_{C_1} = i_{C_2} v_{C_1} = v_{C_2} \quad (5)$$

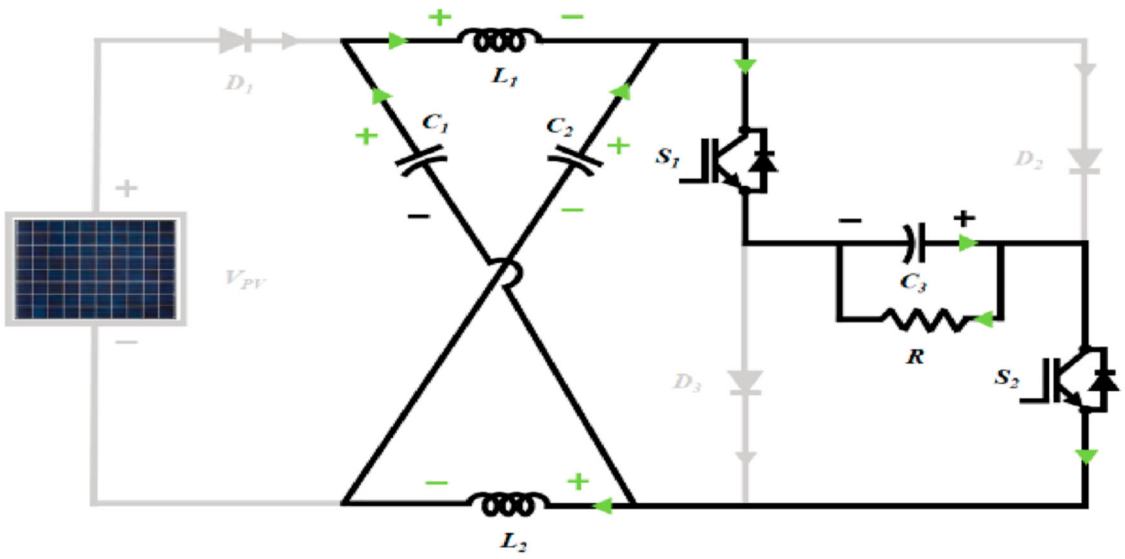

Figure 4. Circuit diagram for current loop in state 1.

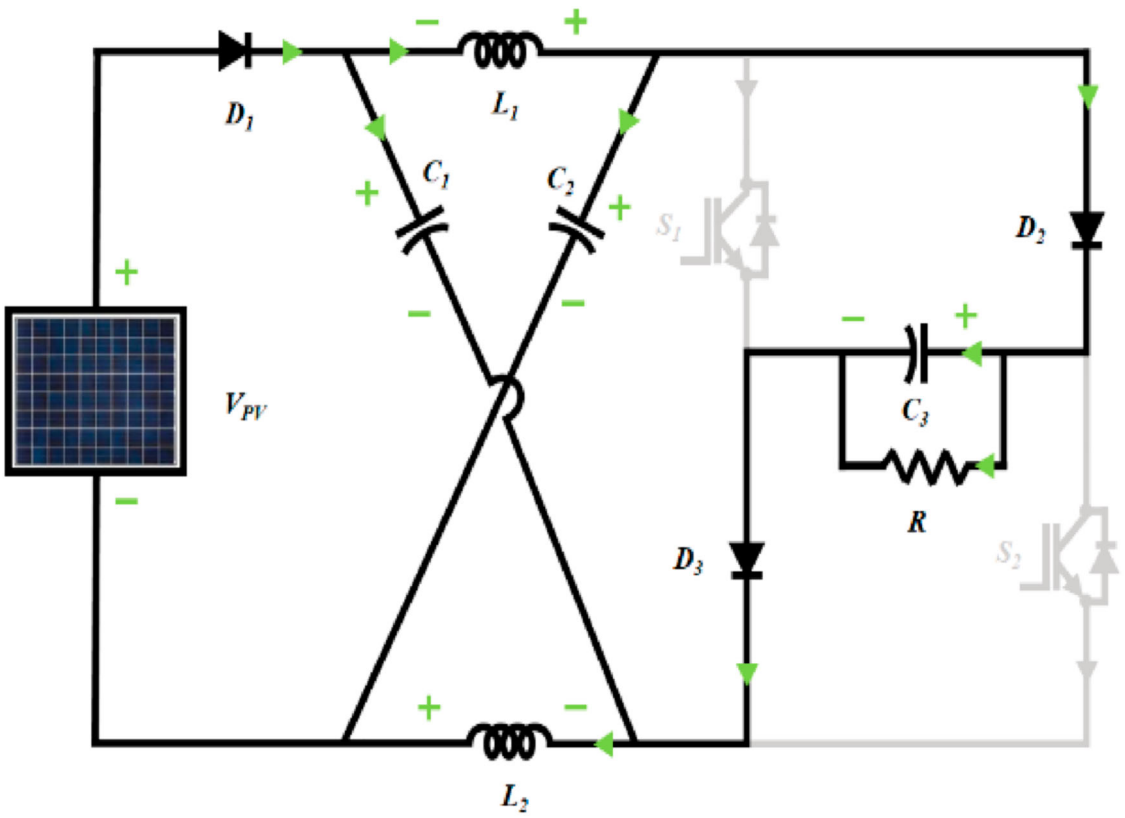

Figure 5. Circuit diagram for current loop in state 2.

Mode 2 in CCM

Mode 2 has states 1, 2 and 3.

State 1$[t_0, t_1]$ and State 2$[t_1, t_2]$: Mode 2 operation is exactly like the two states of mode 1 and in mode 2 at the end of state 2 the operation is different, here the C_3 capacitor is discharged to deliver the load along with the panel voltage which is linked to the series of V_{PV} and the L_1 and L_2 inductors.

State 3$[t_2, t_3]$: The switches S_1 and S_2 and *OFF* and diodes D_1, D_2 and D_3 are*ON* in this state, state 3 voltage relation is equal to state 2, whereas the relation of current is different. The circuit diagram for the current loop in state 3 is shown in Figure 6. Apply KCL in this circuit and the current equation is written as

$$\{i_{D_1} = i_{L_1} - i_{C_1} i_{L_1} = i_{L_2} i_{D_2} = i_{L_1} + i_{C_2} i_{C_1} = i_{C_2} i_{C_3} = i_o - i_{D_3} \quad (6)$$

Mode 3 in CCM

Mode 3 has states 1, 2, 3 and 4.

State 1$[t_0, t_1]$, State 2$[t_1, t_2]$ and State 3$[t_2, t_3]$: Mode 3 operation is exactly like the three states of mode 2 and in mode 3 at the end of state 3 the operation is different, the current flows via the $L_1$and L_2 inductors reach zero and move into the DCM of SZSC. The current flows through inductors L_1 and L_2, capacitors C_1, C_2 and C_3, diodes D_1, D_2 and D_3 and switches $S_1$and S_2 are written as

$$\{i_{L_1} = i_{L_2} = i_{C_1} = i_{C_2} = 0 i_{S_1} = i_{S_2} = i_{D_1} = i_{D_2} = i_{D_2} = 0 i_{C_3} = i_o \quad (7)$$

State 4$[t_3, t_4]$: Switches S_1 and S_2 are in *OFF* and the diodes $D_1, D_2$and D_3 are *OFF*. The voltages remain unchanged over capacitors C_1 and C_2. The circuit diagram for the current loop in state 4 is shown in Figure 7.

3. Closed-loop control with a PI controller using a genetic-based chicken swarm (GBCS) algorithm

The control of the switched boost Z-source converter is achieved by a closed-loop control with a PI controller. The PI controller considerably reduces the steady-state error of the system and proper tuning of the controller is essential. Various algorithms are available for tuning the controller, but the classical procedures result in more settling time with peak overshoot problems. So intelligent-based algorithms are introduced even though these algorithms converge faster, they require more data so optimization algorithms are preferred. In this work, a novel hybrid algorithm is introduced based on the Genetic algorithm (GA) and chicken swarm (CS) algorithm which includes the advantage of both algorithms. The GBCS algorithm is simple with faster convergence which can solve complex problems. A PI controller with proportional gain K_p and integral gain K_i is represented as

$$C(s) = K_p + \frac{K_i}{s} \quad (8)$$

The controller parameters K_p and K_i decide the optimal working of the system and so these parameters are to be optimized. The optimal values for K_p and K_i($K_p = 1$ and $K_i = 0.1$)are chosen such that they minimize the

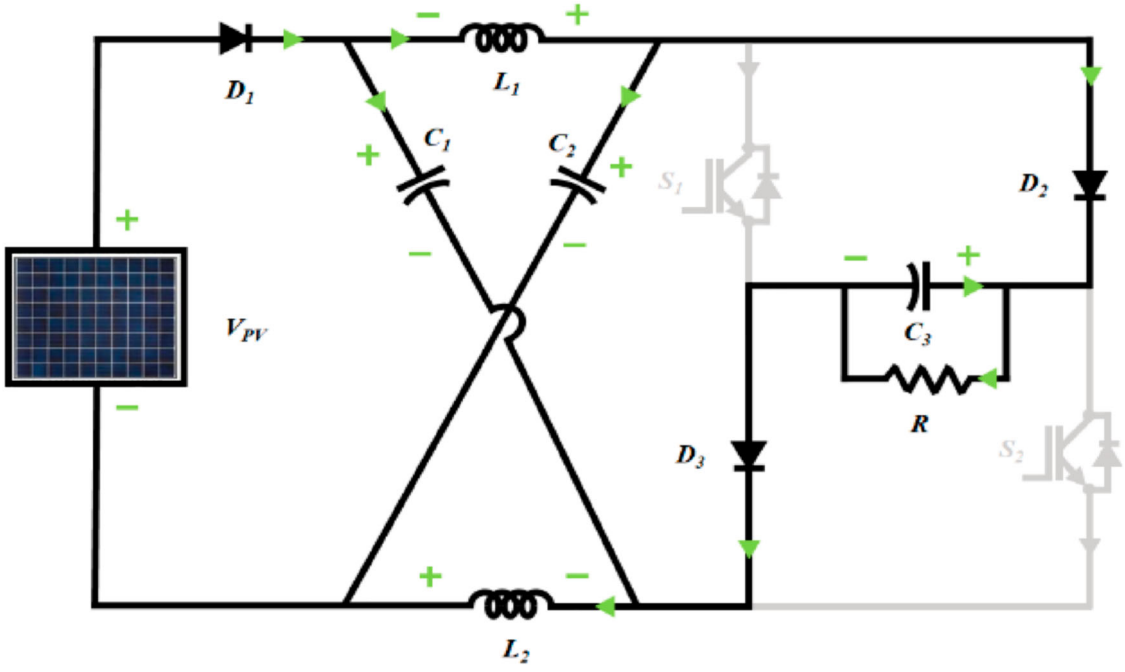

Figure 6. Circuit diagram for current loop in state 3.

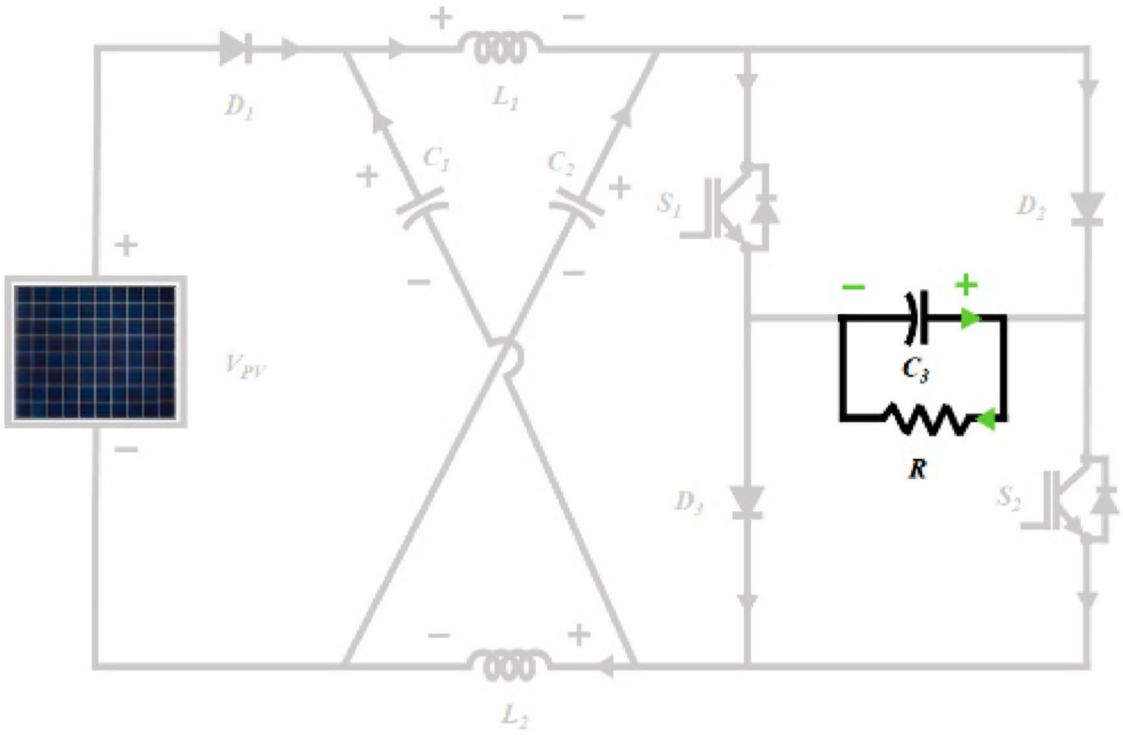

Figure 7. Circuit diagram for current loop in state 4.

error and this is based on the objective function. Mean-square-error (MSE) is expressed mathematically as

$$MSE = \frac{1}{t}\int_0^{\tau} (e(t))^2 \tag{9}$$

The fitness value is thus computed as

$$F = \frac{1}{MSE} \tag{10}$$

The above expression implies that optimal parameters are attained by smaller values of MSE.

One of the global search algorithms that mimic natural selection is the genetic algorithm which is simple and results in optimal solutions. The basic operators of GA are reproduction, cross-over and mutation. The steps involved in GA are as follows:

1. Generate initial population with max. generation limit.
2. Start with the initial population
3. Evaluate the fitness and perform GA operators.
4. Check if the optimal solution is attained. If not, go to the next step
5. If the maximum number of iterations is reached, increase the number of iterations by one and then GA operators are executed, go to step 3

Chicken swarm (CS) optimization

This algorithm is one of the bio-inspired algorithms which mimic the behaviour of a chicken swarm and the lead of the swarm is the rooster followed by hens and chicks. The chicken that has the highest strength is termed a rooster and that with minimum strength is termed a chick. The biological behaviour of chicken to go behind the mother in search of food is the key aspect of this algorithm. Initialization and updating are the two steps in the CS algorithm. During the initialization, the population size and number of roosters, hens and chicks are defined and then the fitness value is evaluated. Each and every member of the group differs, depending on their food-searching capability and based on the fitness value, the food-searching capability of the rooster differs. The formula for updating the rooster's position is given as

$$x_{i,j}^{t+1} = x_{i,j}^{t} \times (1 + randn(0, \sigma^2)) \tag{11}$$

$$\text{If } f_i \le f_k, \text{then } \sigma^2 = 1, \text{or else } \sigma^2 = \exp\left(\frac{(f_k - f_i)}{|f_i| + \varepsilon}\right) \tag{12}$$

where the Gaussian distribution function is denoted by $randn(0, \sigma^2)$ with standard deviation σ^2 and maen 0, fitness value corresponding to x is f, k refers to the rooster's index and zero division error is avoided by introducing a constant σ.

The roosters are followed by hens in search of food and the expression for updating the hen's position is given as

$$x_{i,j}^{t+1} = x_{i,j}^{t} + S_1 \times rand \times (x_{r1,j}^{t} - x_{i,j}^{t}) + S_2 \times rand(x_{r2,j}^{t} - x_{i,j}^{t}) \tag{13}$$

$$S_1 = \exp\left(\frac{f_i - f_{r1}}{abs(f_i) + \varepsilon}\right) \text{ and } S_2 = \exp(f_{r2} - f_i) \tag{14}$$

where $r_1, r_2 \epsilon [1, N]$ such that both are not equal, *rand* is chosen between 0 and 1.

Usually, chicks follow their mothers and the mathematical formulation for updating the chick's position is given as

$$x_{i,j}^{t+1} = x_{i,j}^{t} + FL \times (x_{m,j}^{t} - x_{i,j}^{t}) \tag{15}$$

where the position of the i^{th} mother is denoted by $x_{i,j}^{t}$, *FL* is selected between 0 and 1.

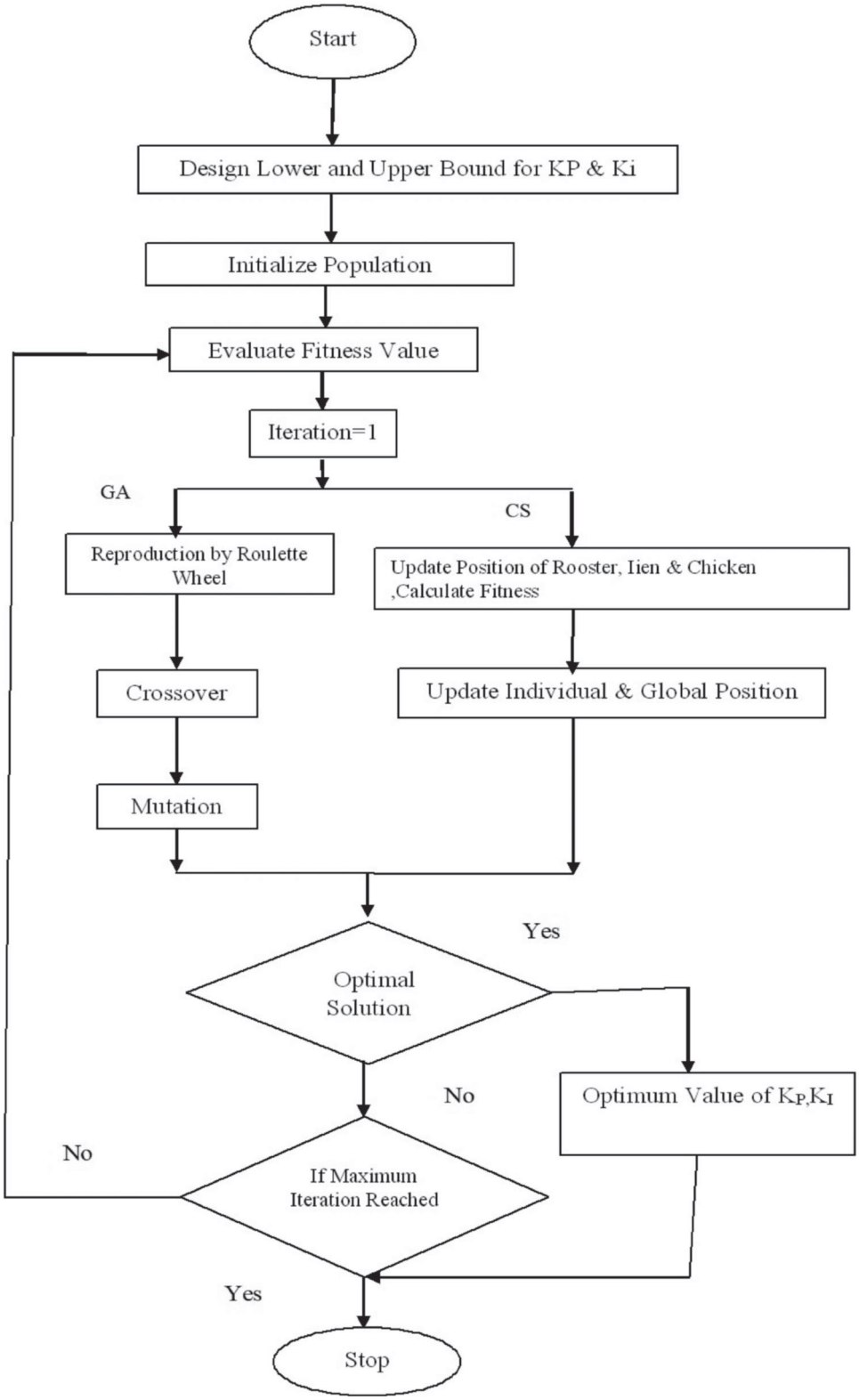

Figure 8. Flowchart for the GBCS algorithm.

GBCS algorithm. This novel hybrid algorithm includes the advantages of both the genetic algorithm and chicken swarm algorithm, such as simplicity, robustness, convergence and the capability of solving complex problems. The flow chart for the hybrid algorithm is illustrated in Figure 8. Initially, the population is generated randomly and the fitness value is evaluated for every solution. After the computation of fitness value, the population is categorized into two subpopulations among which one is updated based on the genetic algorithm and the other is updated based on the chicken swarm algorithm. The new solution generated by each operation is combined in the next generation from which the optimum values for K_p and K_i is attained.

Grid synchronization

To synchronize with the grid, the frequency and phase angle are to be the same. So far, the Phase-locked loop (PLL) is designed to produce a sinusoidal function. The control circuit for grid synchronization is illustrated in Figure 9.

The DC reference current is generated by controlling the DC-link voltage controller, also the load and active current are produced by controlling the PQ controller so the active power which is needed for the grid is calculated. The inverter reference current is obtained by multiplying the load current and required grid current with *sinωt* and this reference is used to control reactive power and THD. Through the PI current controller

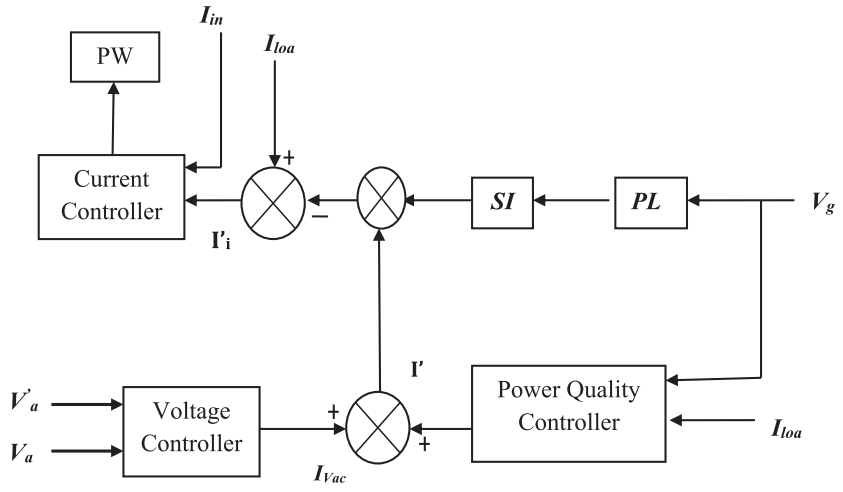

Figure 9. Control circuit for grid synchronization.

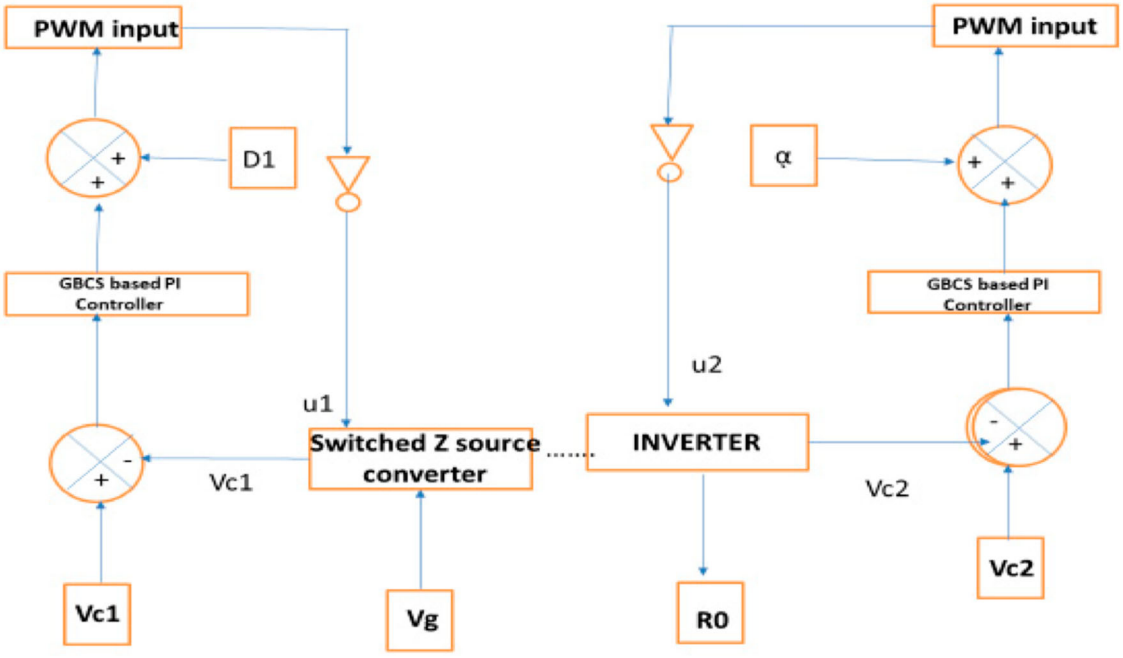

Figure 10. Block diagram of GBCS-based Closed-loop Control.

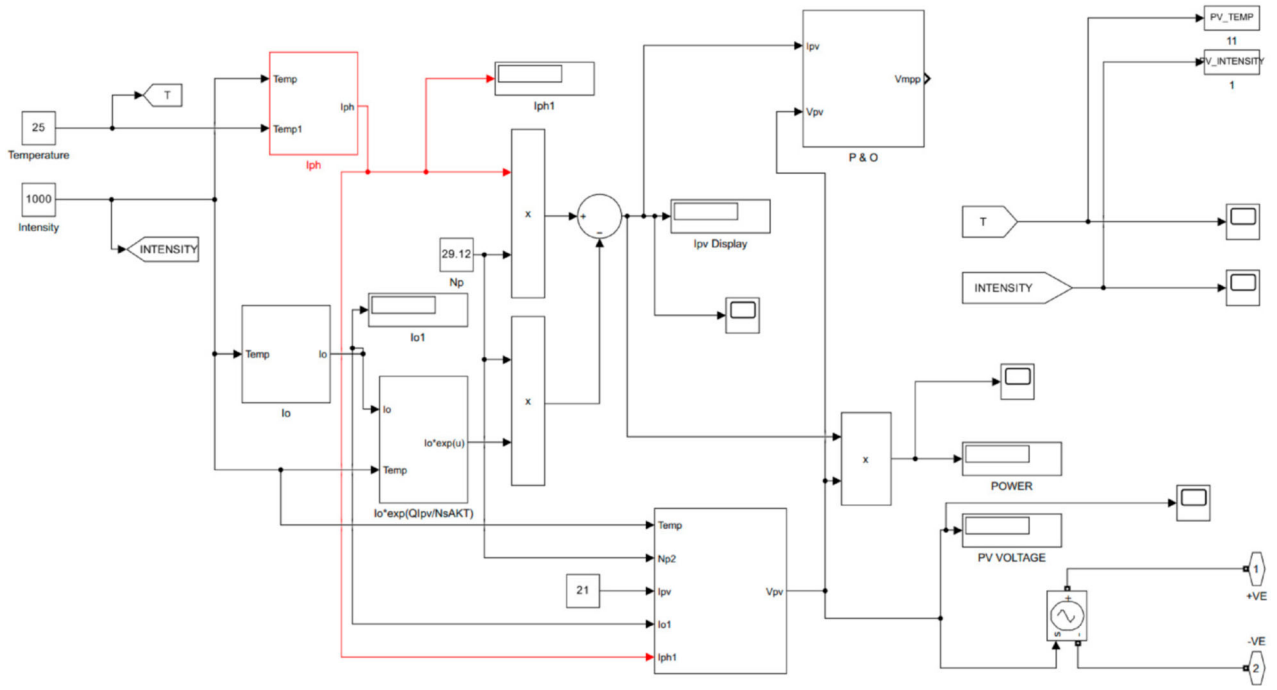

Figure 11. Simulink diagram of PV with MPPT based on the P&O algorithm.

that has the reference current and the actual output current of the inverter as the inputs, the PWM inverter determines the PWM switching pattern (Figures 10 and 11).

4. Results and discussions

The solar array output voltage is fed to a switched Z-source boost converter. In this study, MPPT based on the P&O algorithm is used to maximize power from a PV module. It demonstrates that under rapidly changing irradiance and temperature circumstances, the P&O algorithm offers an effective and reliable maximum power tracking performance. Due to temperature variation, PV panel output link voltage does not maintain a constant value and ripples also occur. The GBCS algorithm-based proportional-integral controller for the proposed converter optimizes the PI controller parameters, thereby retaining the link voltage which reduces ripples and settling time. This voltage is given to the 1Φ grid through 1Φ VSI that converts DC to AC which is controlled by the PI controller. The design of the complete system is validated using MATLAB software and then the designed result is checked with hardware implementation. The solar panel specifications are represented in Table 1. The power rating of 2000W is used.

The specifications for the converter are represented in Table 2. The output voltage of the converter is optimized by the GBCS-PI controller (Table 3).

Simulation results

The simulation results for the photo voltaic integrated grid scheme are accomplished in time scale using Simulink that measures the performance of the converter for a given system. The complete model is obtained from sim-power system toolbox. The PV panel voltage and input current waveform are shown in Figure 12(a,b). From Figure 12(a), it is noted that the PV panel maintains a constant voltage of 80 V which is

Table 1. Specifications for a solar panel.

Components	Ratings/specifications
No. of panel	20
Total no. of series cells	36
Cell area	125 mm × 31.25 mm
Open circuited voltage	21.4 V
Operating voltage	16.8 V
Short circuited current	6.2 A
Operating current	5.8 A
Temperature range	−40 to +85°C
Maximum voltage	1000 V DC

Table 2. Specifications for the converter.

Components	Symbols	Rating
Input voltage	v_{in}	0–120 V
Input current	i_i	20 A (Max)
Capacitor	C_1,C_2	25 uF
Inductor	L_1,L_2	5 mH
Output load current		10 Amps
Operating frequency	f	10 KHZ
Output power	P_0	1500 W
Switches		IRF540
Diodes		MUR1560
Driver circuit		TLP 250

Table 3. Comparison of conventional PI and GBCS PI controllers.

PI controller	GBCS PI controller
Settling Time is 0.25 s	Settling Time is 0.15 s
Currents ripples are high	Current ripples are reduced
THD is 4.3% in Simulink Platform	THD is 1.6% in Simulink Platform
THD is 4.9% in Prototype results	THD is 2.4% in Prototype results

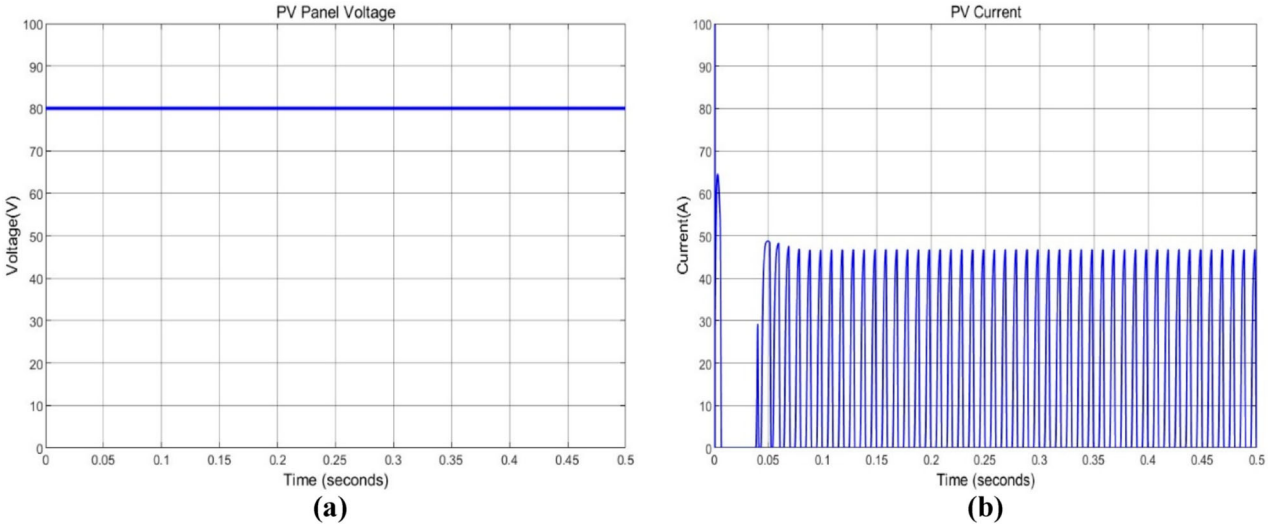

Figure 12. (a) PV panel voltage waveform (b) Input current waveform.

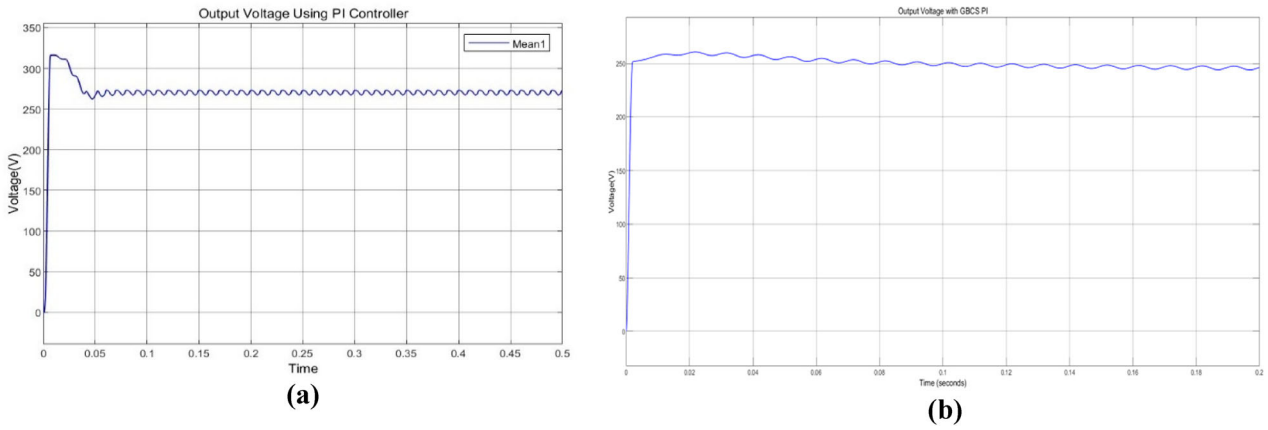

Figure 13. (a) Output DC voltage waveform using the PI controller (b) Converter output voltage waveform using the GBCS-PI controller.

given to the converter as input. Figure 12(b) indicates PV Current which obtains maximum value initially and maintains a constant value of 48A after 0.1 s.

The output DC voltage waveform using the PI controller is depicted in Figure 13(a). From this waveform, it is noted that the voltage does not maintain constant and oscillations also occur. The converter output voltage waveform using the GBCS-PI controller is depicted in Figure 13(b). The voltage output waveforms of the switched Z source Boost converter are shown in Figure 13(b). It shows that even with some early fluctuations, the converter takes 0.15 s to reach its 270 V output voltage. However, the fluctuations are limited using the GBCS-PI Controller.

In Figure 14, the output current is dynamic up to 0.05 s, after which a steady value of 5A is attained.

In Figure 15, the THD waveform is displayed. The THD value of the Z Source Converter is 4.58% which is reduced using the GBCS-PI Controller. The PWM pulses to the converter switches S_1 and S_2 are depicted in Figure 16(a,b). The carrier signal given to the PWM generator generates pulses. These pulses operate the switches S_1 and S_2 that are shown in both waveforms.

The grid voltage and current waveform are shown in Figure 17(a,b). This waveform shows that grid voltage and current are maintained sinusoidal. The harmonics in the inverter current are equal and opposite to that of the load current. The sinusoidal nature of grid current waveform is retained at the fundamental frequency with non-linear load and provides a constant and dependable power supply by remaining steady and free from oscillations. This stability keeps the electrical grid from being disrupted and is essential for the effective operation of linked devices.

The real and reactive power waveform is shown in Figure 18(a,b). The real power waveforminitially decreases and then it attains a maximum power of 1500W after the settling time of 0.04 s it will maintain as constant which is a requirement for the grid. The reactive power waveform initially, it shoots and then decreases. The phase mismatch between the voltage and the current causes oscillations in the reactive power waveform at first, which then settles to a constant. Consequently, the suggested system attained the best possible power flow.

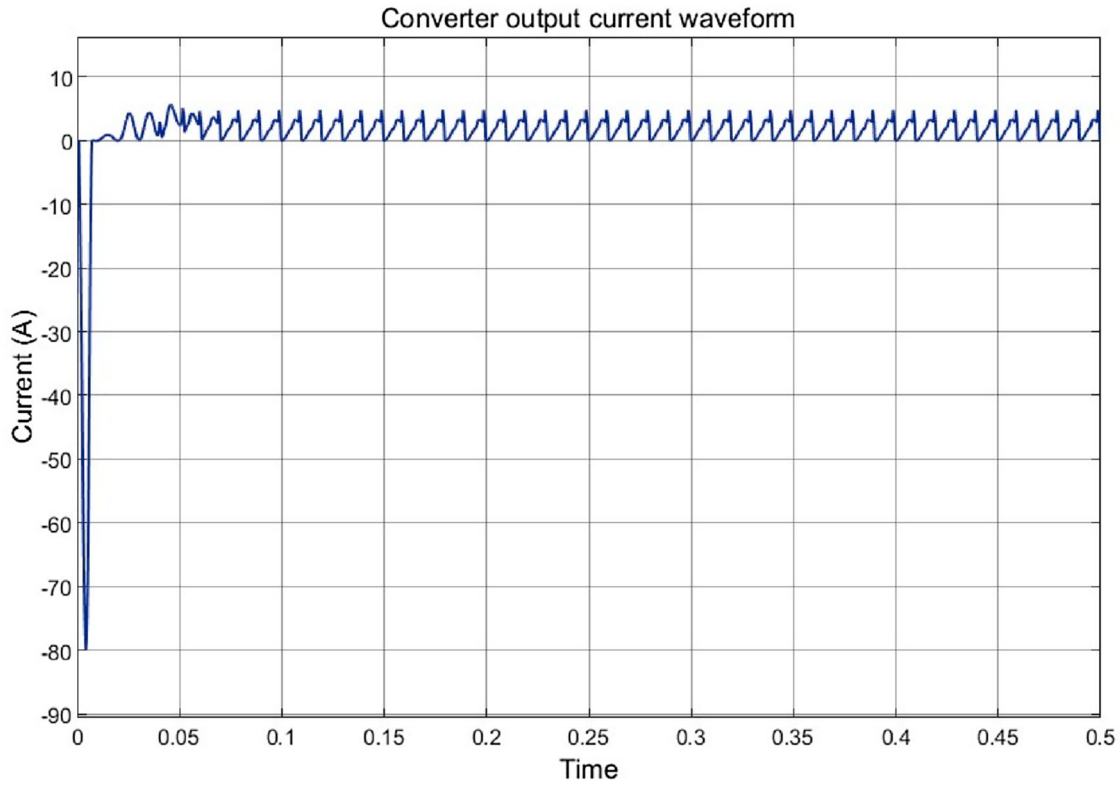

Figure 14. Converter output current waveform.

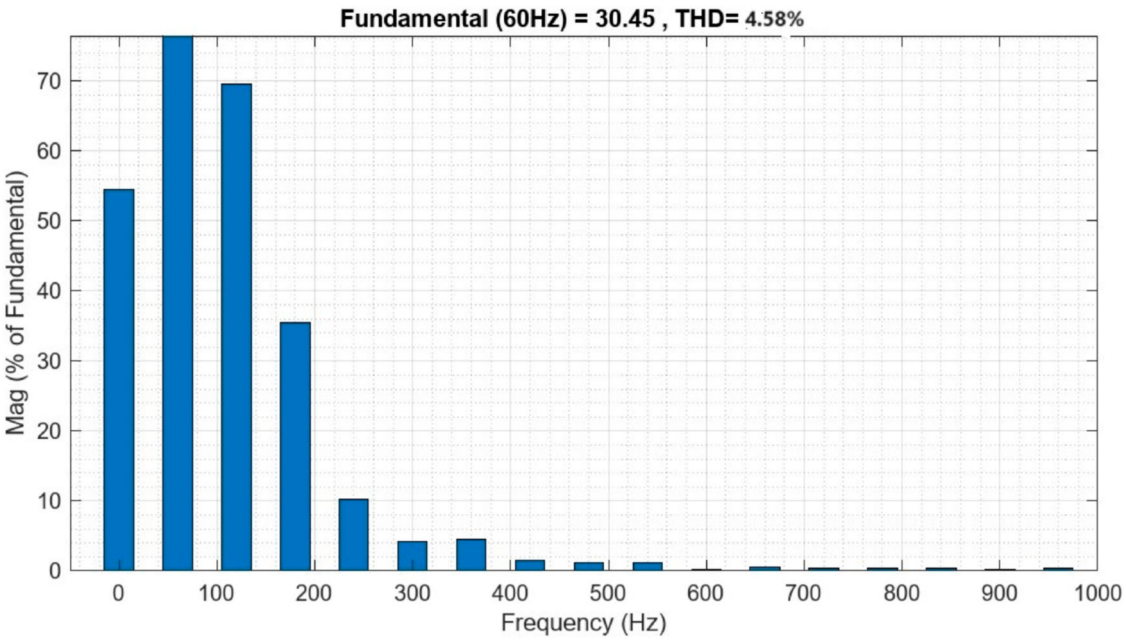

Figure 15. Harmonic analysis of converter output current.

The grid current THD with PI and GBCS-PI is shown in Figure 19(a,b). The behaviour of PI and GBCS-PI controllers is measured by evaluating the grid current THD using a power analyser. It is noted that Grid current THD for the conventional PI controller is 4.3% and the grid current THD for the GBCS-PI controller is 1.6%.

Hardware results

FPGA Spartan 6E is used to develop the proposed converter system prototype is shown in Figure 20. The controller linked with the DC-DC converter uses DC link voltage as a feedback signal. This maintains the converter output in as steady state. The potential divider

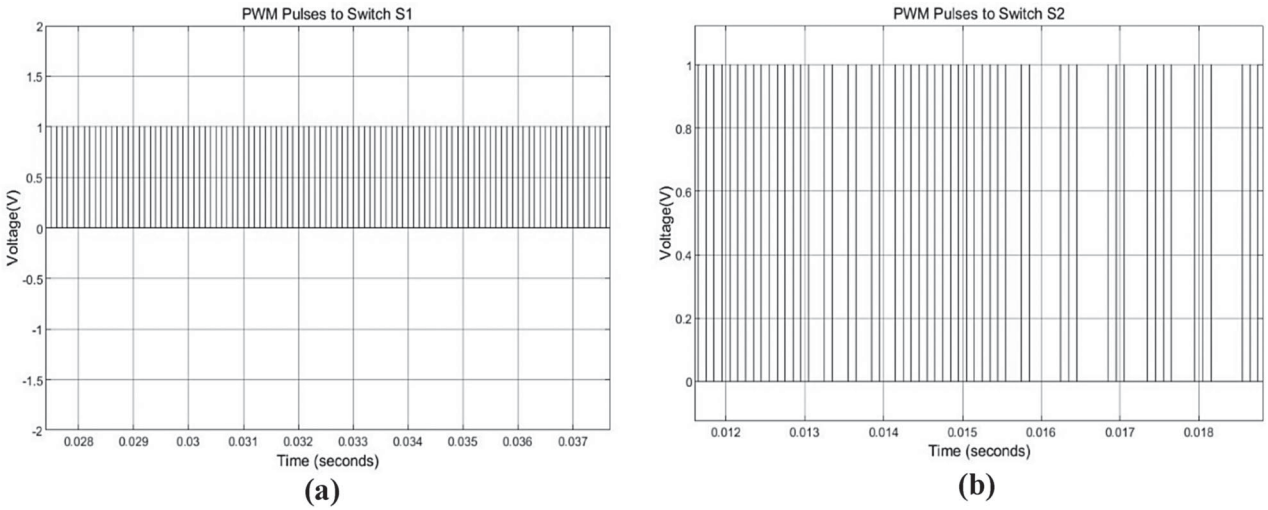

Figure 16. (a,b) PWM pulses to the converter switches $\mathbf{S}_1$ **and** $\mathbf{S}_2$.

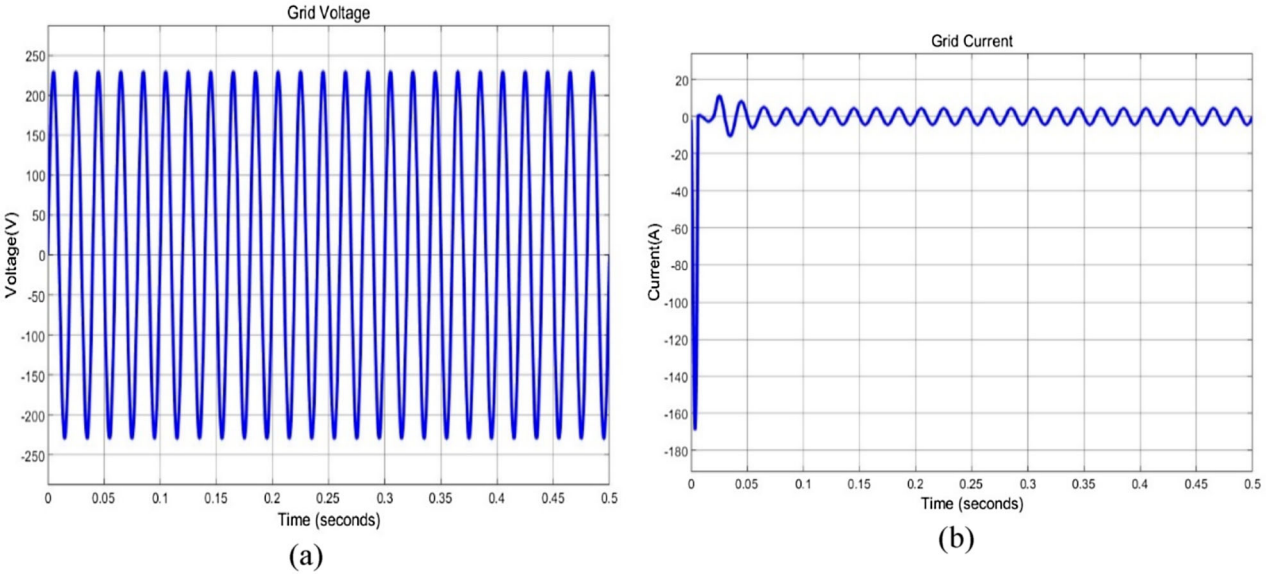

Figure 17. (a,b) Grid voltage and current waveform.

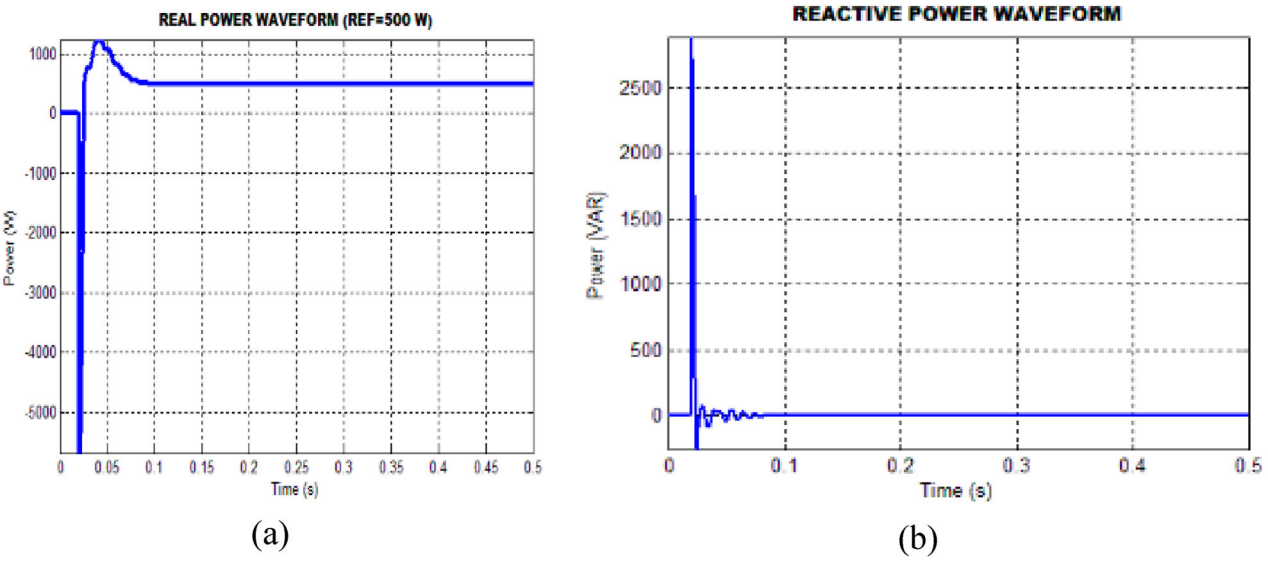

Figure 18. (a,b) Real and reactive power waveform.

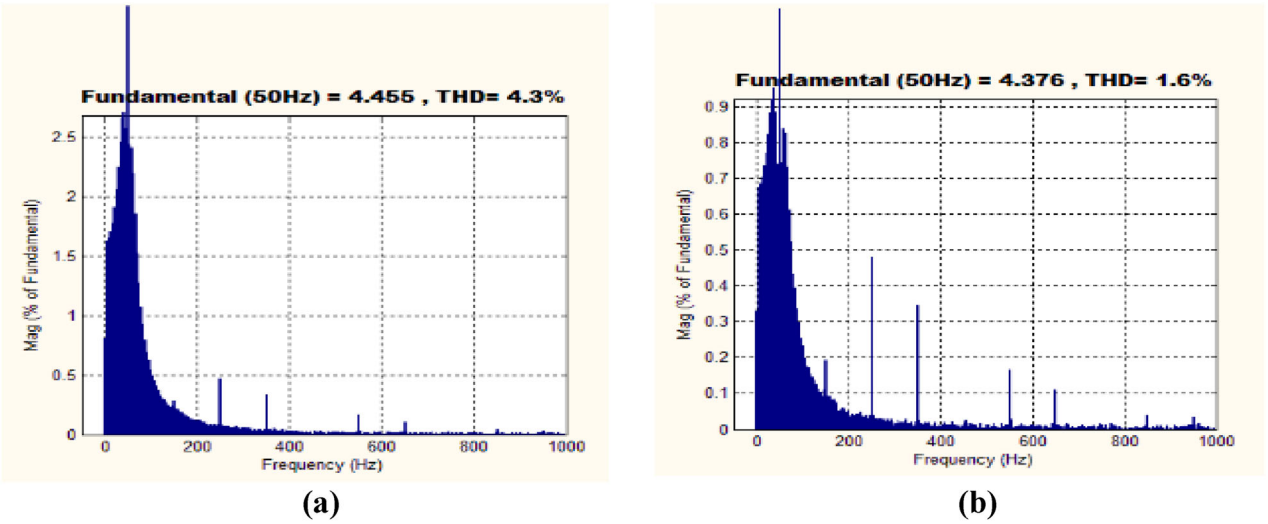

Figure 19. (a,b) Grid current THD with PI and the GBCS-PI controller.

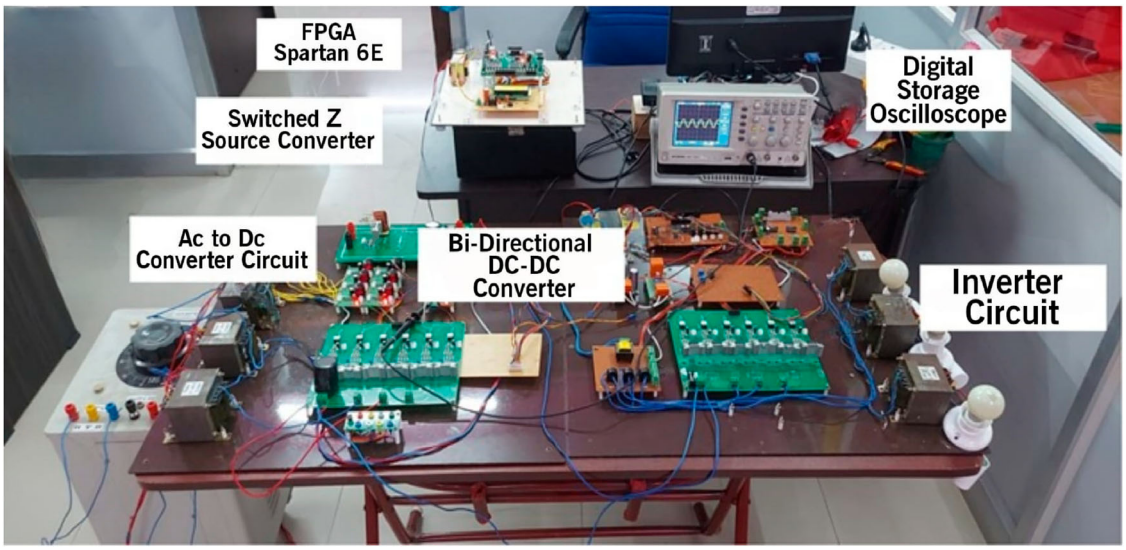

Figure 20. Hardware setup.

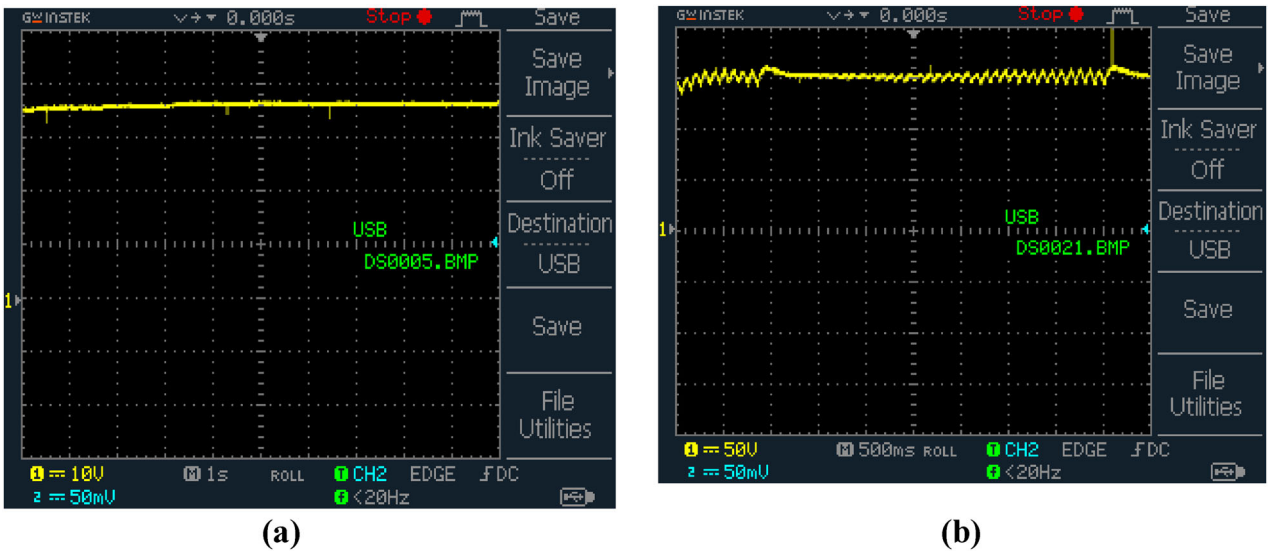

Figure 21. (a,b) Input DC voltage and current waveform.

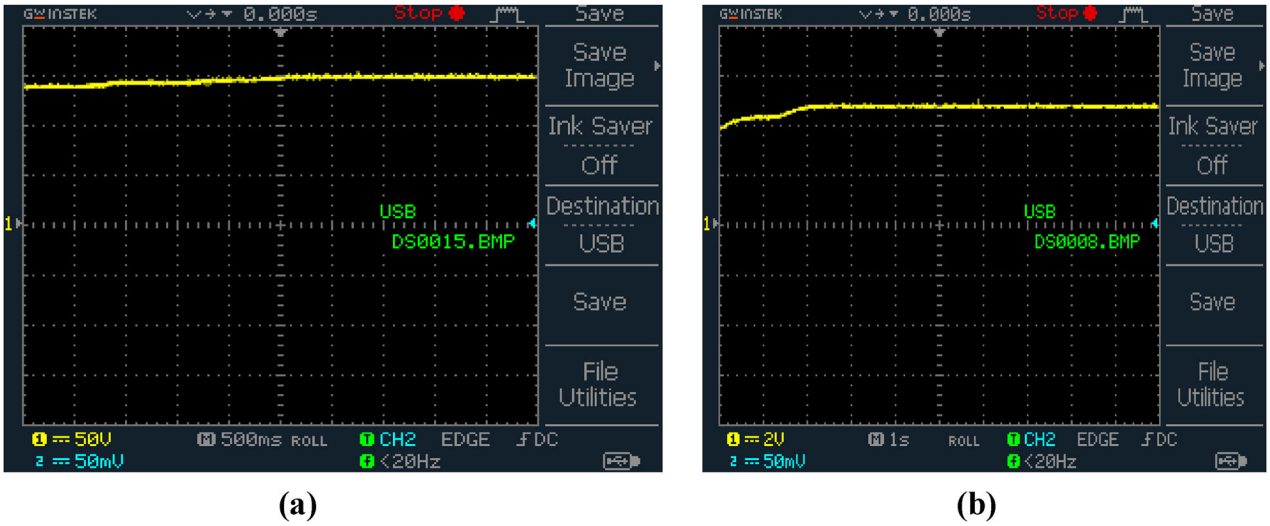

Figure 22. (a) Converter output voltage waveform for the GBCS-PI controller. (b) Output DC waveform.

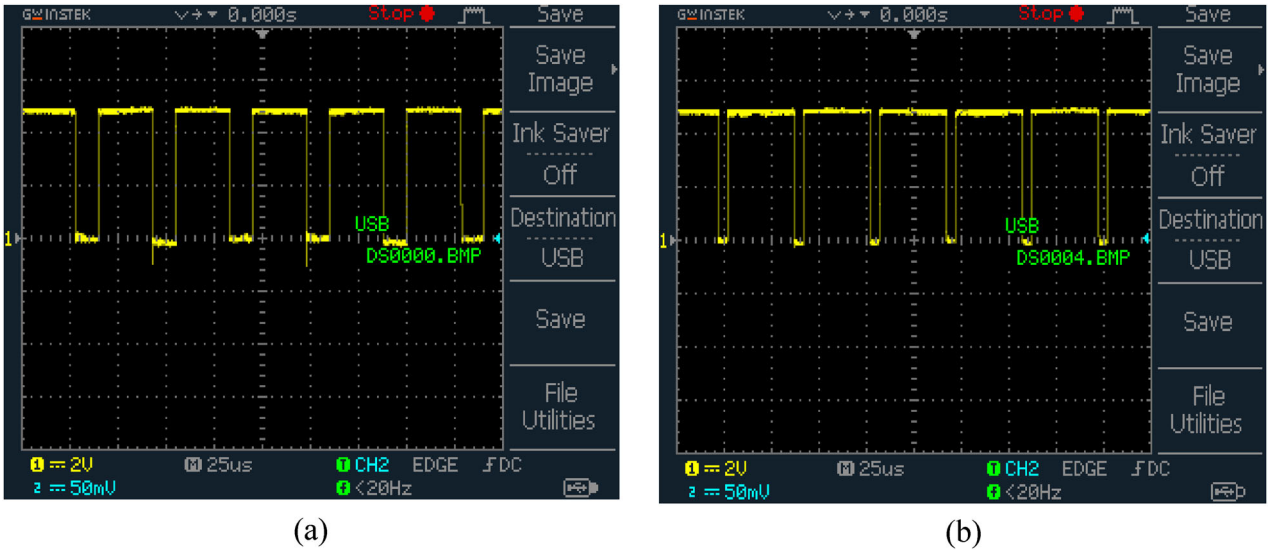

Figure 23. (a,b) Waveform for PWM pulses $\mathbf{S_1}$ **and** $\mathbf{S_2}$.

and the Hall Effect sensor are used to measure real power at the grid. The signals are performed by signal conditioners and then fed to the microcontroller's input point. Using an inbuilt ADC unit, the signals are digitized. The input DC voltage and current waveform are shown in Figure 21. The PV panel output voltage and current waveform are shown. This waveform shows that the variations occur in voltage and current due to temperature changes on the PV array. This is given to the input of the converter.

The converter's output voltage waveform for the GBCS-PI controller is depicted in Figure 22(a). When compared to this waveform with the conventional PI controller, it reduces ripples, reduces maximum peak overshoot, decreases settling time and maintains a constant voltage of 270V DC.

The converter output DC waveform is depicted in Figure 22(b). This waveform shows the output current from the converter.

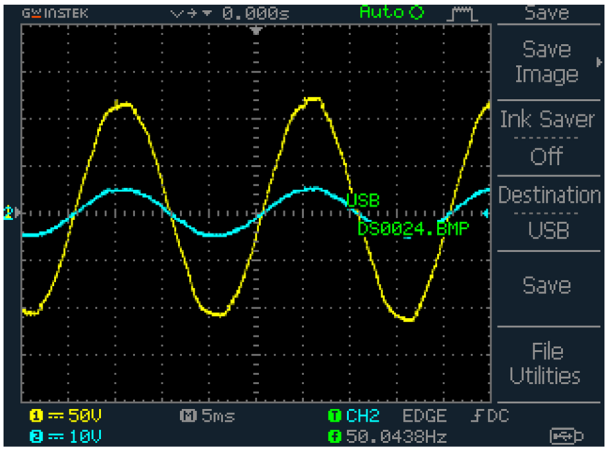

Figure 24. Grid voltage and current waveform.

The PWM pulses to the converter switches S_1 and S_2 are depicted in Figure 23(a,b). The carrier signal given to the PWM generator generates pulses.

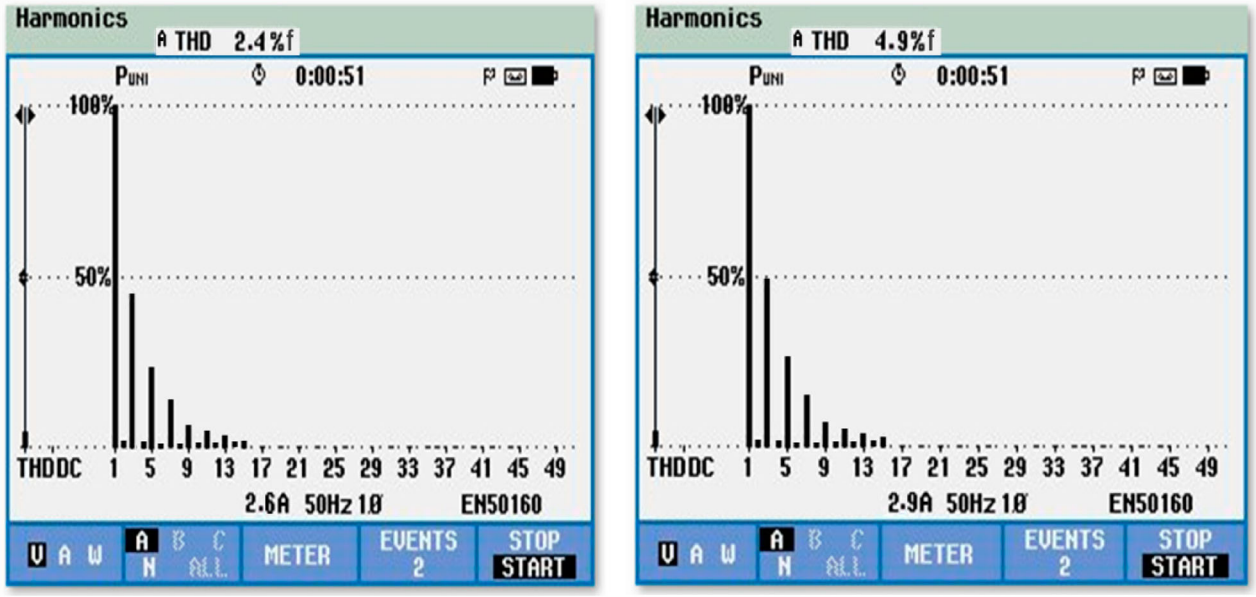

Figure 25. (a,b) THD with GBCS-PI and the PI controller.

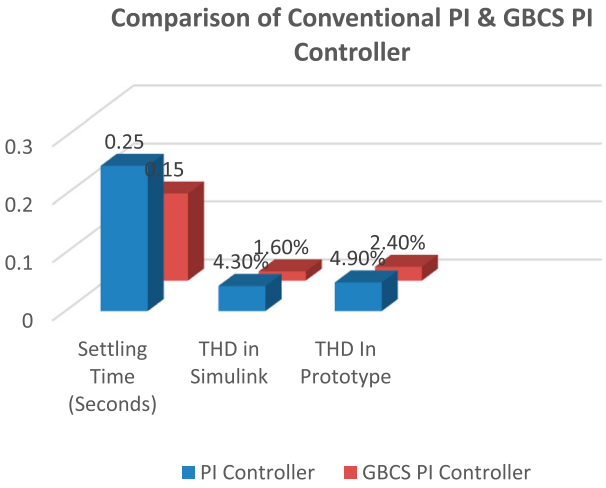

Figure 26. Comparison of GBCS-PI and the PI controller.

The grid voltage and current waveform are shown in Figure 24. The PI controller output is combined with a sine wave reference that is extracted from the power grid and given to the reference power signal.

The THD for GBCS-PI and the PI controller is shown in Figure 25(a,b). It is observed that THD with GBCS-PI obtained is 2.4% and THD with the PI controller obtained is 4.9%. On comparing both THD with GBCS-PI and PI, the GBCS-PI gives better performance (Figure 26).

5. Conclusion

A genetic-based chicken swarm algorithm for PV tied grid with a switched Z-source converter is analysed in this work. The low-voltage output from PV is boosted with the aid of a switched Z-source boost converter with the added advantage of less cost with enriched power quality. The converter is being controlled by a PI controller tuned with genetic-based chicken swarm algorithm which is simpler and more accurate. This converter's output is then fed to the grid through a single-phase VSI and grid synchronization is accomplished with a PI controller in which the actual and reference power are compared and accordingly, pulses are generated for the proper control of the inverter. Thus, the proposed control scheme is verified through simulation in MATLAB and the results are attained. The system's drawback is that grid integration of PV is accomplished with single-phase VSI and switching losses need to be considered. Future research can focus on the converter's bidirectional functioning in grid-connected PV systems and three-phase VSI for grid integration with the consideration of switching losses.

Disclosure statement

No potential conflict of interest was reported by the author(s).

References

[1] Sarita K, Kumar S, Vardhan ASS, et al. Power enhancement with grid stabilization of renewable energy-based generation system using UPQC-FLC-EVA technique. IEEE Access. 2020;8:207443–207464. doi:10.1109/ACCESS.2020.3038313

[2] Chen Q, Wang F, Hodge B-M, et al. Dynamic price vector formation model-based automatic demand response strategy for PV-assisted EV charging stations. IEEE Trans Smart Grid. 2017;8(6):2903–2915. doi:10.1109/TSG.2017.2693121

[3] Kalla UK, Singh B, Murthy SS, et al. Adaptive sliding mode control of standalone single-phase microgrid using hydro, wind, and solar PV array-based generation. IEEE Trans Smart Grid. 2018;9(6):6806–6814. doi:10.1109/TSG.2017.2723845

[4] Saad Al-Sumaiti A, Salama MMA, Konda SR, et al. A guided procedure for governance institutions to regulate funding requirements of solar PV projects. IEEE Access. 2019;7:54203–54217.
[5] Sharma RK, Mishra S. Dynamic power management and control of a PV PEM fuel-cell-based standalone ac/dc microgrid using hybrid energy storage. IEEE Trans Ind Appl. 2018;54(1):526–538. doi:10.1109/TIA.2017.2756032
[6] Zhang X, Hu Y, Mao W, et al. A grid-supporting strategy for cascaded H-bridge PV converter using VSG algorithm with modular active power reserve. IEEE Trans Ind Electron. 2021;68(1):186–197. doi:10.1109/TIE.2019.2962492
[7] Lee HG, Kim G-G, Bhang BG, et al. Design algorithm for optimum capacity of ESS connected with PVs under the RPS program. IEEE Access. 2018;6:45899–45906.
[8] Singh R, Bansal RC, Singh AR, et al. Multi-objective optimization of hybrid renewable energy system using reformed electric system cascade analysis for islanding and grid connected modes of operation. IEEE Access. 2018;6:47332–47354. doi:10.1109/ACCESS.2018.2867276
[9] Pradhan S, Hussain I, Singh B, et al. Performance improvement of grid-integrated solar PV system using DNLMS control algorithm. IEEE Trans Ind Appl. 2019;55(1):78–91. doi:10.1109/TIA.2018.2863652
[10] Malamaki K-ND, Demoulias CS. Estimation of additional PV converter losses operating under PF $\neq 1$ based on manufacturer's data at PF $= 1$. IEEE Trans Energy Convers. 2019;34(1):540–553. doi:10.1109/TEC.2019.2893065
[11] Aghdam FH, Abapour M. Reliability and cost analysis of multistage boost converters connected to PV panels. IEEE J Photovoltaics. 2016;6(4):981–989. doi:10.1109/JPHOTOV.2016.2566885
[12] Azer P, Emadi A. Generalized state space average model for multi-phase interleaved buck, boost and buck-boost DC-DC converters: transient, steady-state and switching dynamics. IEEE Access. 2020;8:77735–77745. doi:10.1109/ACCESS.2020.2987277
[13] Nathan K, Ghosh S, Siwakoti Y, et al. A new DC–DC converter for photovoltaic systems: coupled-inductors combined Cuk-SEPIC converter. IEEE Trans Energy Convers. 2019;34(1):191–201. doi:10.1109/TEC.2018.2876454
[14] Kushwaha R, Singh B. Design and development of modified BL Luo converter for PQ improvement in EV charger. IEEE Trans Ind Appl. 2020;56(4):3976–3984.
[15] Liu J, Wu J, Qiu J, et al. Switched Z-source/quasi-Z-source DC-DC converters with reduced passive components for photovoltaic systems. IEEE Access. 2019;7:40893–40903. doi:10.1109/ACCESS.2019.2907300
[16] Tomar A, Mishra S, Bhende CN. Aomh–MISO based PV–VCI irrigation system using ASCIM pump. IEEE Trans Ind Appl. 2018;54(5):4813–4824. doi:10.1109/TIA.2018.2839728
[17] Uno M, Shinohara T. Module-Integrated converter based on cascaded quasi-Z-source inverter with differential power processing capability for photovoltaic panels under partial shading. IEEE Trans Power Electron. 2019;34(12):11553–11565. doi:10.1109/TPEL.2019.2906259
[18] Li X, Zhu M, Su M, et al. Input-independent and output-series connected modular DC–DC converter with intermodule power balancing units for MVdc integration of distributed PV. IEEE Trans Power Electron. 2020;35(2):1622–1636. doi:10.1109/TPEL.2019.2924043
[19] Li H, Yang D, Su W, et al. An overall distribution particle swarm optimization MPPT algorithm for photovoltaic system under partial shading. IEEE Trans Ind Electron. 2019;66(1):265–275. doi:10.1109/TIE.2018.2829668
[20] Li H, Sun H, Hou L. Adaptive fuzzy PI prescribed performance tracking control for switched nonlinear systems With dead-zone input and external disturbances. IEEE Access. 2020;8:143938–143949. doi:10.1109/ACCESS.2020.3013939